CrystEngComm

PAPER

View Article Online
View Journal | View Issue

Cite this: *CrystEngComm*, 2014, **16**, 4999

A combined experimental-computational study of benzoxaborole crystal structures†

Saad Sene,[a] Dorothée Berthomieu,[a] Bruno Donnadieu,[a] Sébastien Richeter,[a] Joris Vezzani,[a] Dominique Granier,[a] Sylvie Bégu,[a] Hubert Mutin,[a] Christel Gervais[b] and Danielle Laurencin*[a]

Received 11th February 2014,
Accepted 18th March 2014

DOI: 10.1039/c4ce00313f

www.rsc.org/crystengcomm

Benzoxaboroles are organoboron molecules which are gaining growing interest in different fields, notably for the development of new drugs. However, extensive characterization of these molecules in the solid state is still lacking. Here, questions related to the structure and spectroscopic signatures of crystalline benzoxaborole phases are thus addressed, using a combined experimental-computational approach. Two simple benzoxaboroles were studied: 1,3-dihydro-1-hydroxy-2,1-benzoxaborole (denoted as BBzx) and 5-fluoro-1,3-dihydro-1-hydroxy-2,1-benzoxaborole (also referred to as AN2690, a newly developed antifungal drug). First, the crystal structures of AN2690 and BBzx at room temperature are discussed, emphasizing the intermolecular interactions which play an important role in their formation. Then, results of IR and multinuclear (^{1}H, ^{11}B, ^{13}C and ^{19}F) solid state NMR characterization are presented, together with density functional theory (DFT) calculations which were carried out to assist in the interpretation of the spectra. Finally, the influence of polymorphism and anisotropic thermal expansion properties of the crystal structures on the NMR parameters of BBzx and AN2690 is discussed.

1. Introduction

Boronic acids (R–B(OH)$_2$) are a family of molecules which have a wide range of applications.[1] They are commonly used in organic synthesis as reagents in Miyaura–Suzuki coupling reactions,[2] in materials science for the synthesis of sensors[3] or Covalent Organic Frameworks (COFs),[4] and in medicine.[5]

More recently, benzoxaboroles, which are hemi-esters of arylboronic acids, have attracted much attention (Fig. 1).[6–12] Like boronic acids, benzoxaboroles are Lewis acids, which can undergo conversion from trigonal to tetrahedral geometry in the presence of a nucleophile. However, this conversion takes place much more easily than in the corresponding boronic acids, as illustrated for example by the difference in pK_a between phenylboronic acid and the related benzoxaborole (denoted as BBzx, Fig. 1a), with pK_a ~8.9 and pK_a ~7.3, respectively.[1,6,13] This particular reactivity has been the key to the discovery of a series of benzoxaborole-based drugs.[6–9] One of the most studied to date is 5-fluoro-1,3-dihydro-1-hydroxy-2,1-benzoxaborole (AN2690 or "Kerydin" – Fig. 1b), which is a broad-spectrum antifungal drug developed for the treatment of onychomycosis.[6,7,9] Other systematic investigations of benzoxaboroles have been carried out, showing that they have a broad spectrum of potential therapeutic applications.[8,9] For example, AN2728 (Fig. 1c) has interesting properties as a topical anti-inflammatory agent for the treatment of psoriasis and atopic dermatitis,[8a,9] while SCYX-7158 (Fig. 1d, also referred to as AN5568) is being studied for the treatment of human African trypanosomiasis (sleeping sickness).[8b,9]

[a] *Institut Charles Gerhardt de Montpellier, UMR 5253, CNRS-UM2-UM1-ENSCM, Place E. Bataillon, CC1701, 34095 Montpellier cedex 5, France. E-mail: dlaurenc@univ-montp2.fr; Fax: +33 4 67 14 38 58; Tel: +33 4 67 14 38 02*
[b] *Sorbonne Universités, UPMC Univ Paris 06, CNRS, Collège de France, UMR 7574, Chimie de la Matière Condensée de Paris, F-75005, Paris, France*

† Electronic supplementary information (ESI) available: Le Bail refinements of the XRD powder patterns, solution NMR spectra, TGA, comparison of the XRD data and structures of AN2690 and BBzx with those of previously reported structures of these 2 compounds, calculated vibrational modes of AN2690 (PED included) and BBzx, GIPAW calculated NMR parameters for the different reported structures of AN2690 and BBzx, and geometrical features of the different calculated models. CCDC 986106. For ESI and crystallographic data in CIF or other electronic format see DOI: 10.1039/c4ce00313f

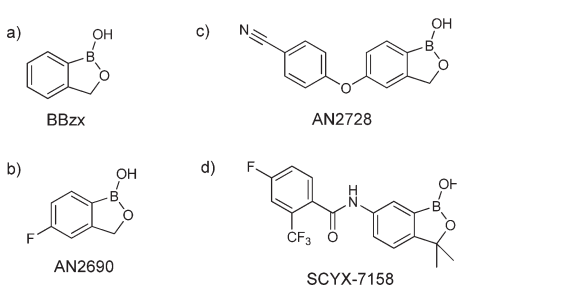

Fig. 1 Examples of benzoxaboroles.

So far, investigations on benzoxaboroles have mainly focused on developing their synthesis, evaluating their reactivity in solution (notably as sugar receptors) or studying their potential therapeutic applications.[6,11a] However, only a handful of benzoxaborole-based structures have been fully characterized in solution and in the solid state.[11a,14–18] To the best of our knowledge, the molecule for which the most spectroscopic data are available is 1,3-dihydro-1-hydroxy-2,1-benzoxaborole (*i.e.* the simplest benzoxaborole, denoted as BBzx in Fig. 1a), whose ^{1}H and ^{13}C NMR spectra in solution and ^{11}B solid state NMR spectrum have been reported.[14,16–18] Density-functional theory (DFT) calculations were also performed on this molecule, notably to calculate Raman and IR vibration modes and ^{11}B NMR parameters.[14,18] In contrast, for other molecules like AN2690, extensive characterizations in the solid state using techniques like solid state NMR are still missing, despite the fact that these could be useful for the analysis of its local environment within complex materials or pharmaceutical formulations, especially in cases where X-ray diffraction analyses are impaired.

Due to the increasing interest in benzoxaboroles, we found it timely to look in more depth not only at their crystal structures but also their spectroscopic signatures in the solid state. In particular, when it comes to pharmaceutical applications, polymorphism is an important point to consider, and a means to distinguish different polymorphs needs to be established.[19] Here, we thus present a comparative study of two benzoxaboroles in the solid state using a combined experimental-computational approach: the antifungal drug AN2690 (Fig. 1b) and its non-fluorinated analogue BBzx (Fig. 1a). The AN2690 phase was synthesized, purified and crystallized as part of this work (as detailed below), while for BBzx, a commercial crystalline phase was studied (after verifying its purity). First, we compare the crystal structures of AN2690 and BBzx in terms of intermolecular interactions. Then, their IR and multinuclear solid state NMR spectra are presented and discussed on the basis of DFT calculations of IR vibrational modes and NMR parameters. Finally, the importance of taking into account temperature effects for the crystalline phases of these benzoxaboroles is discussed, by showing how and why the temperature may affect their spectral properties, notably the solid state NMR ones.

2. Experimental section

2.1 Syntheses

Sodium borohydride ($NaBH_4$, 98+%, Acros Organics), 2-bromo-5-fluorobenzaldehyde (98%, Alfa Aesar), *n*-butyllithium (*n*-BuLi, 2.5 M in hexane, Sigma-Aldrich), triisopropyl borate ($B(O^iPr)_3$, 98+%, AcroSeal, Acros Organics), and 1,3-dihydro-1-hydroxy-2,1-benzoxaborole ($C_7H_7BO_2$, abbreviated here as BBzx, Sigma Aldrich) were used as received. Reagent grade solvents and acids were used in all reactions without further purification, unless specified.

Synthesis of 2-bromo-5-fluorobenzyl alcohol (1). The 2-bromo-5-fluorobenzaldehyde precursor (4.77 g, 23.5 mmol) was dissolved in 80 mL of methanol under magnetic stirring. The solution was cooled to 0 °C using an ice bath. $NaBH_4$ (2.79 g, 73.8 mmol) was then added progressively in order to avoid any excessive effervescence due to the formation of H_2. Once the addition was over, the ice bath was removed and the solution was stirred for 2 hours while gradually warming to room temperature. The progress of the reaction was monitored by thin layer chromatography (silica gel, toluene eluent). The reaction mixture was then slowly acidified with 250 mL of HCl (3 M aqueous solution) and stirred for 15 minutes. The solution was subsequently extracted with diethyl ether (4 × 80 mL). The combined organic fractions were then dried with anhydrous $MgSO_4$ and concentrated. The resulting white powder was dissolved in 100 mL of chloroform. The solution was stirred for 30 minutes, filtered under vacuum in order to remove the insoluble impurities, and finally concentrated. A final purification was performed using silica-gel column chromatography (CH_2Cl_2 eluent), leading to a pure fraction of compound **1** (yield: 88%).

^{1}H NMR (200 MHz, DMSO-d^6): δ 4.49 (d, 2H, J = 5.6 Hz, $-CH_2$), 5.61 (t, 1H, J = 5.6 Hz, –OH), 7,09 (td, 1H, J = 8.9 and 3.3 Hz, H_{ar}), 7,31 (dd, 1H, J = 9.9 and 3.2 Hz, H_{ar}), 7,61 (dd, 1H, J = 8.7 and 5.3 Hz, H_{ar}) ppm.

Synthesis of 5-fluorobenzoxaborole (2) – AN2690. Compound **1** (4.60 g, 22.4 mmol) was dissolved under stirring in 60 mL of anhydrous diethyl ether (the Schlenk flask having been placed initially under a flow of Argon). The solution was cooled to a temperature lower than −30 °C using an acetone–liquid N_2 bath. *n*-BuLi (19 mL, 47.1 mmol) was then added dropwise at a flowrate of 2.7 mL min^{-1} using a syringe pump. After the addition, the solution was stirred for 1 hour. $B(O^iPr)_3$ (6 mL, 24.6 mmol) was then added in the same way. Once the addition was complete, the cooling bath was removed and the solution was stirred overnight under argon while gradually warming to room temperature. The reaction mixture was slowly acidified with 170 mL of H_2SO_4 (2 M aqueous solution) and stirred for 15 min. It was then extracted with diethyl ether (3 × 80 mL). The combined organic fractions were dried with anhydrous $MgSO_4$ and concentrated, leading to the formation of a yellow oil. After one night of slow evaporation at room temperature under air, white crystals formed in the oil. They were isolated by adding 3 mL of toluene (in which AN2690 is less soluble than the impurities), filtering the mixture under vacuum, and then washing the white powder with *n*-pentane. The filtrate was concentrated, leading once more to a yellow oil, in which white crystals formed again after one night under air at room temperature. The same cycle (crystallization–washing–filtration) was thus performed as long as crystals continued to form in the oil. The white solid fractions recovered were combined and a final recrystallization in water at 100 °C was then performed in order to purify compound **2** (yield 45%). At this stage, if traces of boric acid are still present (as seen by ^{11}B NMR), they can be removed by silica gel column chromatography (CH_2Cl_2 eluent). The two steps leading to the formation of AN2690 (compound **2**) are shown

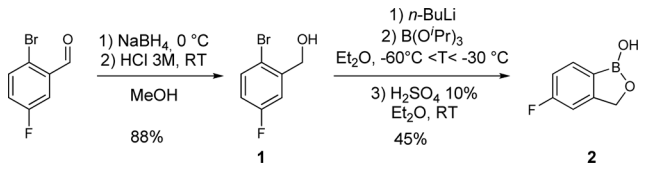

Scheme 1 A two-step synthetic protocol for the preparation of AN2690.

in Scheme 1, and the purification protocol for the second step in Scheme 2.

^{1}H NMR (300 MHz, DMSO-d^6): δ 4.97 (s, 2H, H7), 7.16 (td, 1H, $J_{H-H,H-F}$ = 8.5 Hz, J_{H-H} = 3.2 Hz, H5), 7.25 (dd, 1H, J_{H-F} = 9.7 Hz, J_{H-H} = 3.2 Hz, H3), 7.75 (dd, 1H, J_{H-H} = 8.7 Hz, J_{H-F} = 5.3 Hz, H6), 9.25 (s, 1H, H2) ppm. ^{13}C(^{1}H) NMR (150.9 MHz, DMSO-d^6): δ 69.5 (d, J_{C-F} = 3.1 Hz, C7), 108.5 (d, J_{C-F} = 22.1 Hz, C3), 114.4 (d, J_{C-F} = 22.0 Hz, C5), 132.6 (d, J_{C-F} = 9.3 Hz, C6), 156.6 (d, J_{C-F} = 8.9 Hz), 164.2 (d, J_{C-F} = 246.4 Hz) ppm. ^{11}B NMR (125.4 MHz, DMSO-d^6): 31.8 ppm (s). ^{19}F NMR (282.4 MHz, DMSO-d^6): −110.3 ppm (td, J_{H-F} = 9.6 and 5.9 Hz).

2.2 Characterization

General characterization. IR spectra were recorded in transmission mode on KBr pellets using an Avatar 320 FTIR spectrometer. Thermogravimetric analysis (TGA) measurements were performed on a Perkin Elmer apparatus under air flow with a hold time of 1 min at 25 °C and a temperature increase from 25 to 800 °C at a rate of 5 °C min^{-1}.

X-ray diffraction measurements. X-ray diffraction powder patterns of AN2690 and BBzx were recorded in capillary mode using a PANalytical X'pert MPD-Pro diffractometer equipped with a primary hybrid monochromator block, at the Cu Kα wavelength (λ = 1.5406 Å) (40 kV and 40 mA). Measurements were performed at room temperature between 4° and 70° in 2θ, using a step size of 0.017° and a counting time per step of 600 s. Details on the refinement of the powder diffractograms of AN2690 and BBzx can be found in the ESI.†

A single crystal of AN2690 (0.22 × 0.10 × 0.04 mm) was selected and measured at room temperature (T = 293 K). Measurements were made using an Oxford Diffraction, XCalibur-I four circles kappa-geometry diffractometer, equipped with a large Be window CCD area-detector, using Mo-Kα monochromatized radiation (λ = 0.71073 Å).[20] Intensity measurements were carried out by performing ω scans of Bragg peaks in the range 2.91° < θ <29.01°.

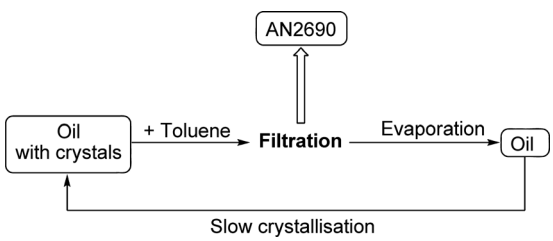

Scheme 2 Procedure for the purification of AN2690.

Experimental intensities were integrated[20] from several series of exposures; the total data set was a sphere. An empirical absorption correction was then applied using spherical harmonics implemented in a SCALE3 ABSPACK scaling algorithm.[21]

Structure resolution of the single crystal XRD data of AN2690. The structure was solved by using direct methods[22] and subsequent differences Fourier maps, then refined by least squares procedures on weighted F^2 values using SHELXL-97,[23] as included in the WinGx system programs for Windows (WinGX version 2013.3 – July 2013).[24] All non-hydrogen atoms were assigned anisotropic displacement parameters and refined without positional constraints. Hydrogen atoms were constrained to ideal geometries and refined with fixed isotropic displacement parameters. Least squares refinement proceeded smoothly to give the residuals shown in Table 1.

Solution NMR experiments. ^{1}H NMR spectra were recorded using Bruker 300 or 200 MHz NMR spectrometers at frequencies of 300.13 and 200.13 MHz, respectively. ^{19}F NMR spectra were recorded using a Bruker 300 MHz NMR spectrometer operating at a frequency of 282.40 MHz. The ^{13}C NMR and 2D ^{1}H–^{13}C HMQC (Heteronuclear Multiple-Quantum Correlation) NMR spectra were recorded using a Bruker 600 MHz NMR spectrometer operating at a ^{13}C frequency of 150.94 MHz. ^{11}B NMR spectra were recorded using a Bruker 400 MHz NMR spectrometer at a frequency of 128.38 MHz.

Solid state NMR experiments. All solid state NMR experiments were performed using a Varian VNMRS 600 MHz (14.1 T) NMR spectrometer. A 3.2 mm Varian T3 HXY magic angle spinning (MAS) probe was used for ^{1}H, ^{13}C and ^{11}B experiments, while a 2.5 mm Varian T3 HFXY probe was used for ^{19}F experiments. The operating frequencies for ^{1}H, ^{13}C, ^{11}B and ^{19}F were 599.82, 150.83, 192.44 and 564.33 MHz, respectively. All NMR experiments were performed under temperature regulation in order to ensure that the temperature inside the rotor is 20 °C (except for the variable-temperature ^{19}F NMR studies mentioned in the discussion).

Windowed-DUMBO[25] ^{1}H-MAS experiments were carried out at a spinning speed of 10 kHz. The RF field strength was 100 kHz, the duration of one DUMBO element was 34.4 μs, and the observation window was 0.8 μs. Four transients were acquired with a recycle delay of 1024 s for AN2690 and BBzx (in both cases, the recycle delay chosen corresponds to full ^{1}H relaxation). A scaling factor was applied to the frequency axis to ensure its accurate calibration. ^{1}H chemical shifts were referenced to external adamantane at 1.8 ppm (used as a secondary reference).

^{1}H–^{13}C CPMAS NMR spectra were recorded spinning at 20 kHz, using a contact time of 2.5 ms (ramped pulse), and 100 kHz spinal-64 ^{1}H decoupling during acquisition. A recycle delay of 128 s was used for AN2690 and BBzx. A total of 320 and 106 transients were recorded for AN2690 and BBzx, respectively. ^{13}C chemical shifts were referenced externally to adamantane (used as a secondary reference); the high frequency peak was set to 38.5 ppm.

Table 1 Crystallographic data and structure refinement for AN2690

CCDC	986106
Structure	Single crystal
Empirical formula	$C_7H_6BFO_2$
M_r/g mol^{-1}	151.93
Temperature/K	293(2)
λ/Å	0.71073
Crystal system	Triclinic
Space group	$P\bar{1}$
a/Å	4.0277(2)
b/Å	6.3237(6)
c/Å	14.0649(14)
α/°	97.110(8)
β/°	91.015(6)
γ/°	100.632(7)
V/Å^3	349.07(5)
Z	2
ρ_{calc}/g cm^{-3}	1.445
μ/mm^{-1}	2.984
F(000)	1764
ω_{min}–ω_{max}/°	2.91 to 29.01°
Index ranges	$-5 \le h \le 5$; $-7 \le k \le 7$; $-17 \le l \le 17$
Reflns collected	8573
Independent reflns	1413 (R_{int} = 0.0197)
Completeness to θ = 29.2°	99.9%
Absorption correction	Empirical correction
Max. and min. transmission	0.9743 and 0.9953
Refinement method	Full-matrix least-squares on F^2
Data/restraints/parameters	1413/0/100
Goodness-of-fit on F^2	S = 1.044
R indices [for 2890 reflections with $I > 2\sigma(I)$]	R_1 = 0.0370, wR_2 = 0.0906
R indices (for all 3693 data)	R_1 = 0.0480, wR_2 = 0.0976
Weighting scheme [where $P = (F_o^2 + 2F_c^2)/3$]	Calc w = $1/[s^2(F_o^2) + (0.0461P)^2 + 0.060P]$
Largest diff. peak and hole	0.150 and −0.166 e Å^3

^{11}B MAS NMR spectra were recorded spinning at 20 kHz MAS. The single pulse experiments were performed with a ~45° solid pulse of 1.25 μs and 100 kHz spinal-64 ^{1}H decoupling during acquisition. A recycle delay of 100 s was used for AN2690 and 32 s for BBzx (corresponding in both cases to full relaxation of ^{11}B). A total of 50 and 340 transients were recorded for AN2690 and BBzx, respectively. ^{11}B chemical shifts were referenced to external $NaBH_4$ at −42.05 ppm (used as a secondary reference).

The ^{19}F MAS NMR spectrum of AN2690 was recorded spinning at 20 kHz. The single pulse experiment was performed with a 90° pulse of 2.5 μs and 80 kHz CW (continuous wave) ^{1}H decoupling during acquisition. A recycle delay of 60 s was used and a total of 4 transients were recorded. ^{19}F chemical shifts were referenced to external commercial PTFE at −122.4 ppm (used as a secondary reference).

2.3 Computational details

Models. Density functional theory calculations were carried out on two types of models: molecular models and periodic unit cell models. Molecular models were used to assist in the interpretation of the IR spectrum of AN2690, while periodic unit cell models were used to determine how IR and solid state NMR spectroscopy can be used to distinguish the different crystalline forms of AN2690 and BBzx.

DFT calculations on molecular models. Molecular models of BBzx and AN2690 were studied, both as single molecules and dimers. It should be noted that DFT calculations were also carried out on a fluorobenzene molecule (C_6H_5F), as mentioned later in the manuscript.

Geometry optimizations and IR frequency calculations were carried out within the *ab initio* Gaussian code,[26] using the hybrid B3LYP functional,[27] and an all-electron Gaussian basis set 6-311++g(d,p). SCF convergence was set to 10^{-8} for the energy during geometry optimisation and frequency calculations.

Normal mode analyses were made using the potential energy distribution (PED), calculated according to previous studies,[28,29] using the hessian matrix calculated by the B3LYP/6-311++g(d,p) method. Only contributions larger than 10% were considered for simplicity. A set of ($3N$ − 6) Wilson–Decius coordinates (N = number of atoms) was used and combined to take into account symmetries, such as cycle symmetries. IR absorption intensities were calculated from the atomic polar tensors.[26,30]

DFT calculations on periodic unit cell models. DFT calculations were carried out on the crystalline structures of the different crystalline forms of BBzx and AN2690, described as infinite periodic systems using periodic boundary conditions. The unit cell parameters and symmetry were set according to the experimental single-crystal XRD data, and

kept fixed during the geometry optimizations. Experimental atomic positions were used as a starting point for the geometry, and then relaxed by DFT.

Geometry optimization was performed using the VASP,[31] Crystal09[32] and/or QUANTUM-ESPRESSO (QE)[33] codes. The different combinations of calculation codes, functionals and basis sets tested on the two forms of AN2690 are summarized in Table 2. For the Crystal09 calculations, SCF convergence was set to 10^{-7} and 10^{-10} for the energy during geometry optimisation and frequency calculations, respectively. For the VASP and QE calculations, the positions of all atoms were relaxed until the total energy difference between the loops was less than 10^{-4} eV and 10^{-10} Ry, respectively. It should be noted that the number of *k*-points used for the VASP calculations on AN2690 was set to 36 (4 × 4 × 4 grid), as no significant difference in energy was observed for a higher number of *k* points (5 × 5 × 5 grid). The Grimme correction[34] was included in some of the calculations to take into account the weak dispersion forces, because in the systems studied here, Van der Waals interactions are particularly relevant in describing intermolecular forces. Calculations including the Grimme correction are referred to as B3LYP-D* (Crystal 09).[35]

First principles calculations of NMR parameters were carried out using the GIPAW method (Gauge Including Projector Augmented Wave)[40] on the structures obtained after geometry optimization using the QE code. The GIPAW method is indeed increasingly being used in materials science to calculate the NMR parameters of organic, inorganic and hybrid materials.[41,42] The wave functions are expanded on a plane wave basis set with a kinetic energy cut-off of 80 Ry. The integral over the first Brillouin zone was performed using a Monkhorst-Pack 4 × 4 × 4 *k* point grid. The isotropic chemical shift δ_{iso} is defined as $\delta_{iso} = -[\sigma - \sigma_{ref}]/[1 - \sigma_{ref}]$ where σ is the isotropic shielding and σ_{ref} is the isotropic shielding of the same nucleus in a reference system (as previously described).[43] The principal components V_{xx}, V_{yy}, and V_{zz} of the electric field gradient (EFG) tensor, defined as $|V_{zz}| \geq |V_{xx}| \geq |V_{yy}|$, are obtained by diagonalisation of the tensor.

Table 2 Periodic DFT calculation methods for geometry optimizations of AN2690 forms

Code	Functional	Basis Set
Crystal09 (ref. 32)	B3LYP	BS-A[a,b]
"	B3LYP-D*	BS-A[a,b]
"	B3LYP	BS-A[a,c]
"	B3LYP	BS-B[c,d]
"	PBE	BS-B[c,d]
VASP[31]	GGA-PBE[e]	BS-C[f]
QE[33]	GGA-PBE[e]	BS-D[g]

[a] BS-A: all electron Gaussian basis-set for B: 621/21/1; for C: 621/21/1; for O: 631/31/1; for F: 6211/411/1; and for H: 31/1. [b] Five tolerances setting the accuracy of the mono and bi-electron integrals: 8 7 7 8 25. [c] Five tolerances setting the accuracy of the mono and bi-electron integrals: 6 6 6 6 12. [d] BS-B: pob-TZVP.[36] [e] PBE-generalised gradient approximation.[37] [f] BS-C: valence electrons described by PAW pseudopotentials.[38] [g] BS-D: valence electrons described by norm conserving pseudopotentials[39a] in the Kleinman Bylander[39b] form.

The quadrupolar interaction can then be characterized by the quadrupolar coupling constant C_Q and the asymmetry parameter η_Q, which are defined as $C_Q = eQV_{zz}/h$ and $\eta_Q = (V_{yy} - V_{xx})/V_{zz}$. The *Q* values reported by Pyykkö were used in these calculations.[44] For the ^{19}F chemical shift calculations, the reference system was fluoroapatite and a scaling factor $k = 0.8$ was applied, in line with recent GIPAW calculations on ^{19}F.[45]

3. Results and discussion

3.1 Synthesis and purification of AN2690

Different strategies have been described in the literature for the synthesis of AN2690.[7a,15,46,47] The most common route uses 2-bromo-5-fluorobenzaldehyde as a precursor. Baker *et al.*,[7a] who were the first to describe the synthesis of AN2690 starting from this precursor, obtained the pure product after 4 steps (reduction–protection of the alcohol–cyclisation–deprotection) with ~60% overall yield. Similar synthetic routes were then used by Ding *et al.*[47] and Gunasekera *et al.*[46] who optimized the reaction and reduced it to 2 steps with ~40% and ~65% overall yield, respectively.

The methodology we decided to use here to synthesize AN2690 was the one described by Gunasekera *et al.*[46] which presents the advantage of being a practical procedure for large scale syntheses of benzoxaboroles. It involves 2 steps: (i) reduction of 2-bromo-5-fluorobenzaldehyde and (ii) one-pot reaction with NaH, *n*-BuLi and $B(O^iPr)_3$, followed by acid treatment of the reaction medium and column chromatography to purify the product. Our attempts to reproduce this synthesis led to overall yields ~25%, much lower than those reported in the literature (~65%). Thus we adapted the procedure in order to try to increase the yield.

Concerning the first step, which is the reduction of the fluorinated benzaldehyde using $NaBH_4$, we noticed the presence of an impurity that was insoluble in chloroform, which was identified as $B(OH)_3$ by ^{11}B MAS NMR. We found that it can be successfully eliminated by washing the product with chloroform, as boric acid is poorly soluble in this solvent, and then performing a silica gel column chromatography. In doing so, the alcohol (compound **1**) used in the next step is pure.

In order to further improve the yield in the second step, which is the most critical, Et_2O was first replaced by THF. However, the excessive formation of insoluble unidentified products was observed in the reaction mixture, indicating that THF is a less appropriate solvent. The procedure was then tested using Et_2O as a solvent, but avoiding the use of NaH, which was replaced by *n*-BuLi for the deprotonation and debromination of the alcohol (Scheme 1). After acidic treatment and extraction with Et_2O, a yellow oil was obtained. At this stage, column chromatography was first performed in order to purify the product, but it led to a very small amount of the pure product, because in several of the fractions collected from the column, AN2690 was found to remain mixed with other impurities. For better purification, we developed a new strategy after having observed that crystals of AN2690

form in the crude oil (see Scheme 2 and Experimental section). The desired compound AN2690 was thus obtained in 40% overall yield after a final recrystallization step in water. Although this is still lower than the one reported by Gunasekera *et al.*,[46] it is nevertheless the best we could achieve starting from 2-bromo-5-fluorobenzaldehyde. Most importantly, no impurities were observed by ^{1}H, ^{13}C, ^{11}B and ^{19}F solution NMR, and Le Bail refinements of the XRD data recorded on the microcrystalline powder of AN2690 also confirmed its purity (see Fig. S1 in the ESI†).

The solution NMR spectra of AN2690 can be found in the supporting information, together with those of the non-fluorinated analogue, BBzx (Fig. S2 and S3 in the ESI†). All resonances were assigned unambiguously (Tables S1 and S2 in the ESI†), and the J coupling values were determined based on previous NMR studies of fluorinated aromatics.[48] The spectra reported here for AN2690 and BBzx are consistent with those already published in the literature,[15,17,46] with the assignments of the ^{13}C resonances of AN2690 being proposed here for the first time. It should be noted that in agreement with previous observations, the ^{13}C signal of the carbon linked to boron is significantly broadened, and thus barely observable on the ^{13}C solution NMR spectra.

3.2 Characterization in the solid state

AN2690 and BBzx were characterized in the solid-state using X-ray diffraction, IR and solid state NMR spectroscopy, as well as TGA. Below, XRD, IR and NMR results are successively discussed, while TGA data can be found in the ESI† (Fig. S4).

X-ray diffraction. The XRD powder patterns of AN2690 and the commercial BBzx phase, both recorded in capillary mode, are shown in Fig. 2. In both cases, the diffractograms were compared to those simulated from the crystal structures previously reported for these two compounds (ESI,† Fig. S5).[49]

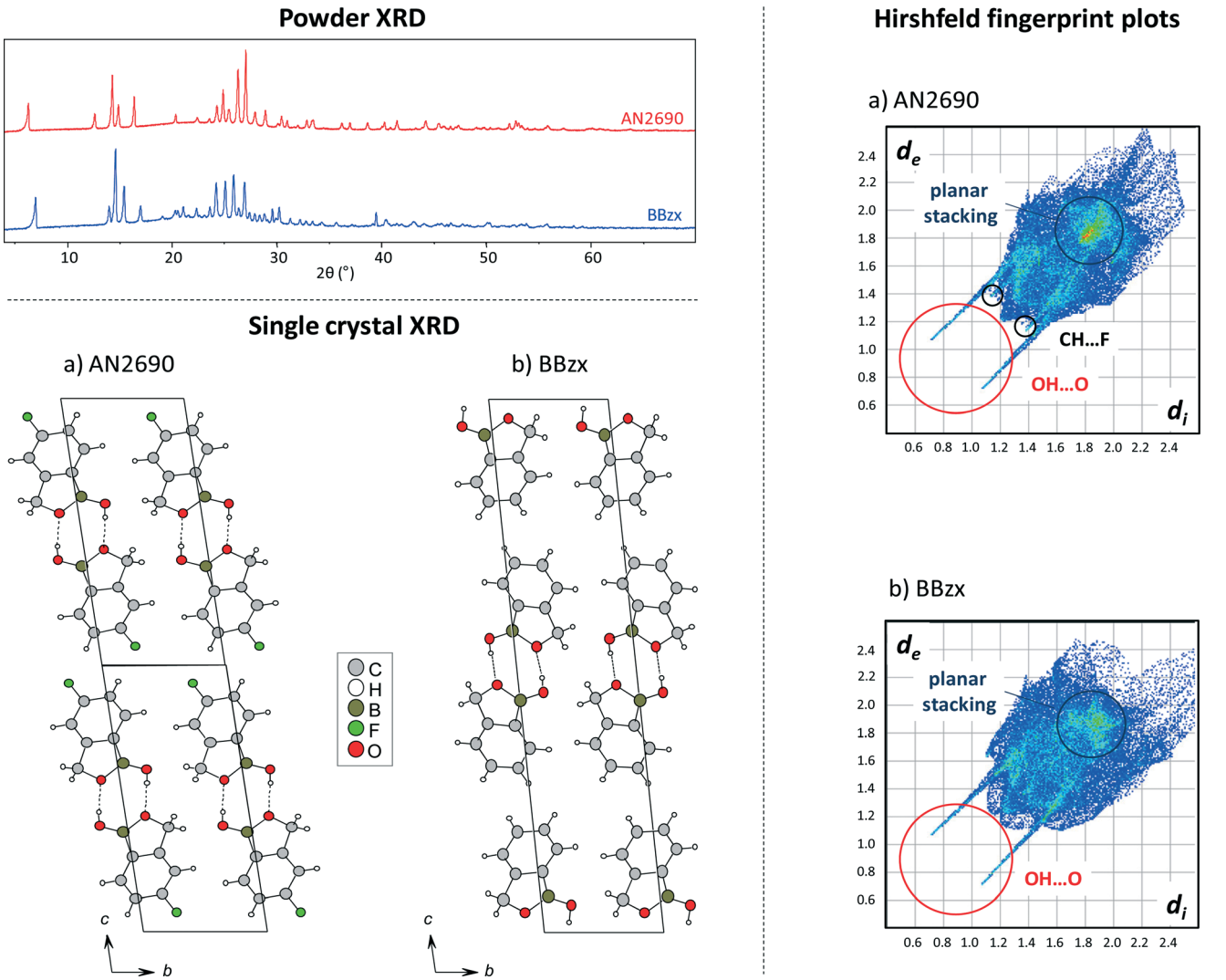

Fig. 2 Top left: XRD powder patterns of AN2690 (red) and BBzx (blue) recorded at room temperature. Bottom left: crystal structures of AN2690 and BBzx (polymorph P(1)),[16] corresponding to the crystalline phases studied here. Right: Hirshfeld surface fingerprint plots of AN2690 and BBzx (polymorph P(1)). On the Hirshfeld surface fingerprint plots, d_e is the distance from a point on the Hirshfeld surface to the nearest nucleus outside the surface, while d_i is the distance from a point on the surface to the nearest nucleus inside the surface.[50]

In the case of AN2690, the XRD pattern of the microcrystalline powder we had synthesized was different from the one expected based on the crystal structure previously reported by Madura *et al.*[15] Le Bail refinements were thus performed on the experimental diffractogram of AN2690 (Fig. S1 in the ESI†), and a single crystal of sufficient quality was also isolated, which was analyzed by single-crystal XRD analysis. The new structure is essentially the same as the previously reported one: same space group, similar lattice parameters, and similar positioning of the molecules in the unit cell (ESI,† Table S3 and Fig. S6). Thus, the discrepancy in the powder patterns is not due to the formation of a new polymorph of AN2690, all the more since the Hirshfeld surface fingerprint plots of both forms of AN2690 are nearly identical (ESI,† Fig. S7).[50] The differences in their powder patterns may rather result from the fact that XRD measurements were not performed at the same temperature (293 K for us *vs.* 100 K for Madura *et al.*),[15] and that AN2690 undergoes an anisotropic thermal expansion. Indeed, the *a* lattice parameter increased by nearly 4% between both measurements, while *b* and *c* varied by less than 0.5%. It should be noted that examples of anisotropic thermal expansion have been reported previously for molecular crystals,[51] and the importance of taking them into account in the pharmaceutical context has been emphasized.[51a]

In the case of BBzx, two different polymorphs have been reported in the literature. The crystal structure of BBzx was first described by Zhdankin *et al.*[16] who found that this molecule can crystallize in the triclinic $P\bar{1}$ space group, with two independent molecules in the unit cell (polymorph referred to as P(1)). Another polymorph (referred to as P(2)) was then obtained for this molecule by Adamczyck-Wozniak *et al.*,[17] with a monoclinic $P2_1$ space group and also two independent molecules in the unit cell. The packing of the molecules in both polymorphic forms is very similar (see the ESI,† Fig. S8). Here, Le Bail refinements on the experimental powder pattern recorded at room temperature show that it corresponds to the P(1) polymorph (see the ESI,† Fig. S1), with only slightly different lattice parameters compared to the previously published structure, due to the difference in temperature in the measurements (293 K for us *vs.* 173 K for Zhdankin *et al.*). However, it is worth noting that the cell parameters vary much less with temperature compared to those of AN2690. In the course of our study, no single crystal of BBzx of sufficient quality could be isolated to record and solve a room-temperature structure.

Many similarities appear between the structures of AN2690 and BBzx. As shown in Fig. 2, both are composed of benzoxaborole dimers, which interact with each other through H bonds, and then pile through weaker π-stacking interactions, perpendicularly to the aromatic cycles. In the case of AN2690, the presence of a fluorine atom leads to additional C–H···F interactions with neighbouring aromatic cycles (shortest intermolecular C–H···F distance is ~2.6 Å). It has been shown that such interactions, although of weak energy, can contribute to the crystal packing.[52] The comparison of the Hirshfeld surface fingerprint plots of AN2690 and BBzx (Fig. 2, right) finely makes evident the different intermolecular interactions mentioned above, with notably the signature of OH···O hydrogen bonds, and evidence of the C–H···F close contacts. Concerning AN2690, the differences in intermolecular interactions along and perpendicularly to the (*bc*) plane may perhaps be related to the anisotropy in its thermal expansion. Indeed, it appears that the thermal expansion is the strongest when it is perpendicular to the (*bc*) plane, *i.e.* where the weakest intermolecular interactions (*i.e.* interplanar stacking) occur.

IR spectroscopy. The IR spectra of AN2690 and BBzx are shown in Fig. 3. These are in agreement with the crystal structures, with the presence of a broad O–H stretching band centered at ~3300 cm^{-1}, due to the H-bonding in the solid-state. Indeed, as mentioned above, the crystal structures of BBzx and AN2690 are both formed of benzoxaborole molecules facing each other and interacting through H-bonds.

To assist in the interpretation of the other IR vibration bands, DFT calculations were carried out on molecular models of both structures, composed of either a single molecule of AN2690 and BBzx, or of dimers of these molecules (involving H-bonds). A similar approach had previously been proposed in the literature for the study of the vibrational modes of benzoxaboroles.[17] The geometry of the dimers, after optimization, is very similar to the one adopted by the molecules in the solid state (see the ESI,† Table S4, for AN2690). The analysis of the calculated vibration frequencies for BBzx and AN2690 was then performed (see the ESI,† Tables S5 and S6). After the comparison of the experimental and calculated vibration frequencies, and of the Potential Energy Distribution (PED) analysis of the calculated vibrational modes (see ESI), it appears clearly, for example, that the C–F stretching frequency for AN2690 is observed at 1250 cm^{-1} on the experimental IR spectrum, the calculated frequency being ~1264 cm^{-1} for the dimer model. It is worth noting that (i) the ν_{C-F} frequency calculated for AN2690 is of the same order of magnitude as those of other molecules like fluorobenzene (ν_{C-F}(calc) = 1235 cm^{-1}), making the assignment of this vibration band unambiguous; (ii) the vibrational mode at 1264 cm^{-1} in the dimer is actually composite, with the C–F

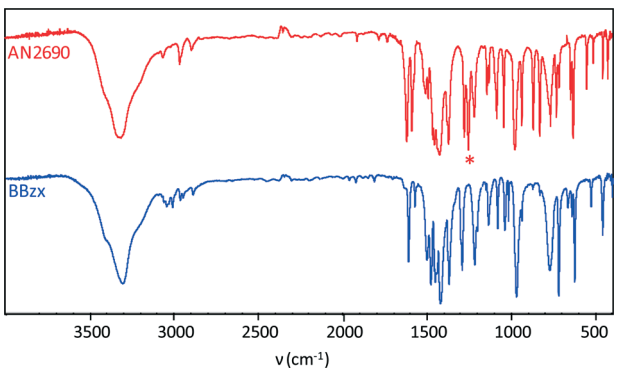

Fig. 3 IR spectra of AN2690 (red) and BBzx (blue). The "*" symbol indicates the C–F stretching frequency of AN2690.

stretching representing only 20% of the mode (see the PED analysis in the ESI†); and (iii) when the periodic model of this structure is considered (not just the dimer), a similar value was found for the calculated C–F frequency (ν_{C-F}(calc) = 1275 cm^{-1}).

Solid state NMR. Multinuclear solid state NMR characterizations were then performed on AN2690 and BBzx (Fig. 4) in order to extract experimental ^{1}H, ^{13}C, ^{11}B (and ^{19}F) NMR parameters. To assist in the interpretation of the spectra, GIPAW calculations were carried out on periodic models of the structures shown in Fig. 2,[53] The calculated NMR parameters can be found in Tables 3 and 4.

The ^{1}H NMR spectra are shown in Fig. 4a. Using homonuclear decoupling during the acquisition (the DUMBO scheme), it was possible for both molecules to resolve resonances coming from the methylene groups between 4.0 and 5.0 ppm. In the case of AN2690, a lower resolution is achieved due to the additional ^{1}H···^{19}F dipolar coupling, which results in a strong overlap of the signals of aromatic and hydroxyl protons between ~5.2 and ~8.2 ppm. Concerning BBzx, a better resolution is obtained in this area of the spectrum and two groups of signals can be distinguished. Based on the GIPAW calculations (Tables 3 and 4, and Fig. S9 in the ESI†), the signals between ~5.2 to ~6.5 ppm correspond to aromatic protons only, while those between ~6.5 to ~8.2 ppm correspond to both aromatic and hydroxyl protons of BBzx. Finally, it should be noted that for both AN2690 and BBzx, the high chemical shifts of the hydroxyl protons are consistent with the presence of strong H-bonds in the solid state.[54]

In the ^{13}C CPMAS NMR spectra, finely resolved ^{13}C resonances were observed (Fig. 4b). The signals which can be easily assigned are those of the CH_2 group, which is centered at ~70 ppm for both molecules, and the carbon linked to the fluorine, which is centered at ~166 ppm for AN2690 and split in two due to the ^{13}C–^{19}F J coupling. The other signals were assigned by comparison with the solution ^{13}C NMR spectra and confirmed by the GIPAW calculations (Tables 3 and 4, and Fig. S10 in the ESI†). In contrast with solution NMR, the carbon linked to the boron is observable in the solid state;[55] it is clearly resolved in the case of AN2690 (centered at ~123 ppm), while it overlaps with other ^{13}C resonances in the case of BBzx (centered at ~130 ppm). Concerning BBzx, it should be noted that most of the signals of the two crystallographically independent molecules cannot be resolved by 1D ^{13}C solid state NMR, a result which is not fully surprising given the GIPAW calculated ^{13}C chemical shifts (which are

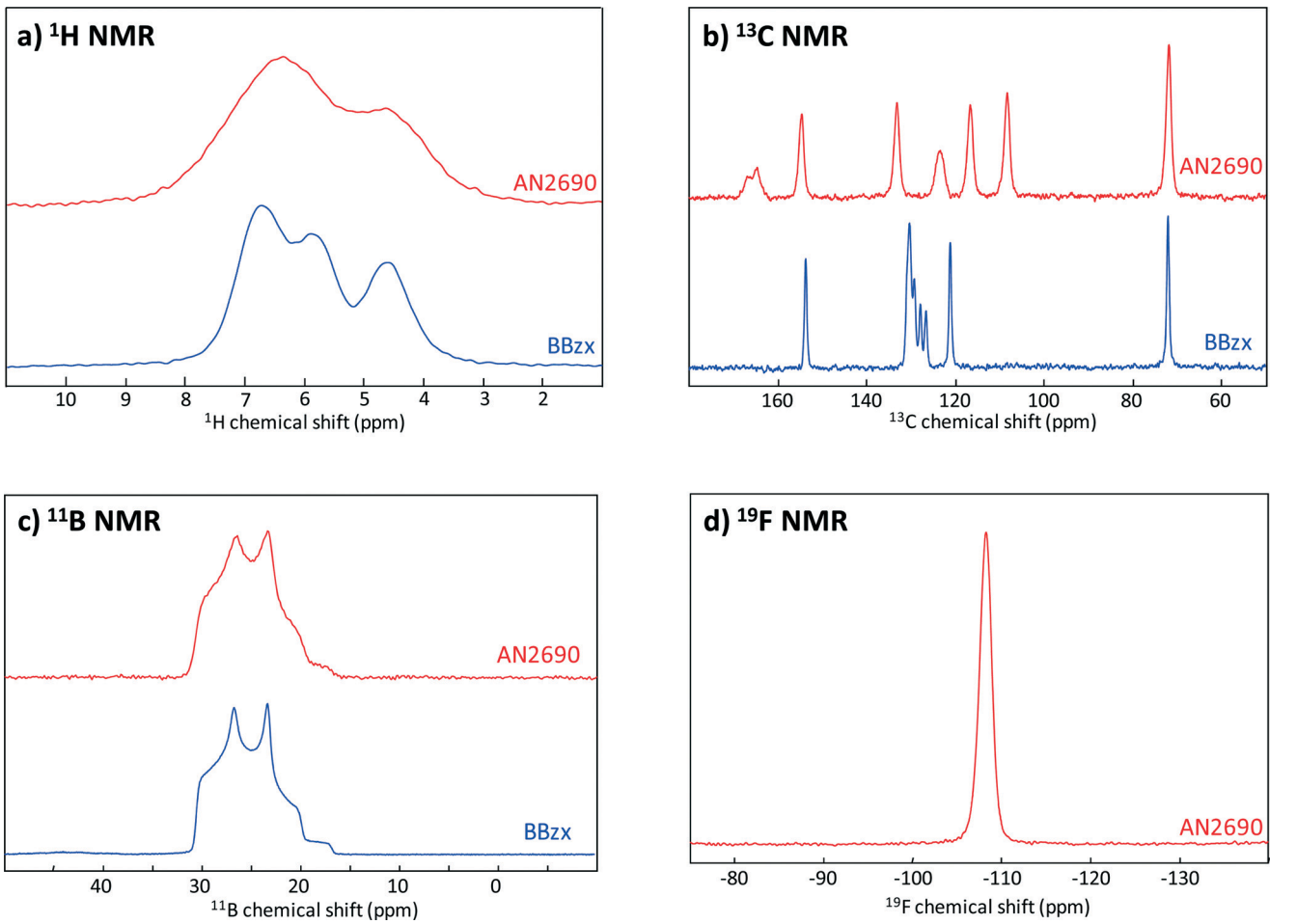

Fig. 4 ^{1}H, ^{13}C, ^{11}B and ^{19}F solid state NMR spectra of AN2690 (red) and BBzx (blue).

Table 3 Experimental and calculated NMR parameters for AN2690. Calculated values reported here are those obtained for the structure solved at 293 K (after VASP DFT relaxation of the atomic positions)

^{1}H NMR			^{13}C NMR			^{11}B NMR							^{19}F NMR		
	δ_{iso} (ppm)			δ_{iso} (ppm)			δ_{iso} (ppm)		C_Q (MHz)		η_Q			δ_{iso} (ppm)	
H	Exp	Calc	C	Exp[a]	Calc	B	Exp[a]	Calc	Exp[a]	Calc[b]	Exp[a]	Calc	F	Exp	Calc
—	—	—	C_1	123.6	126.1	B_1	31.1	32.3	2.8	3.26	0.51	0.59	F_1	−108.6	−109.7
H_2	5 to 8	8.0	C_2	154.6	159.7										
H_3		6.5	C_3	108.3	110.6										
—	—	—	C_4	165.7	174.8										
H_5	5 to 8	6.2	C_5	116.6	118.9										
H_6		6.9	C_6	133.2	136.4										
H_{7A}	4 to 5	4.4	C_7	71.8	74.9										
H_{7B}		4.9													

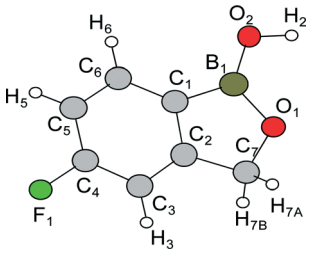

[a] Estimated experimental errors are ~0.2 ppm for δ_{iso}(^{13}C) and δ_{iso}(^{19}F), ~0.1 ppm for δ_{iso}(^{11}B), ~0.02 MHz on C_Q(^{11}B) and ~0.03 for η_Q(^{11}B). [b] Using the scaling factor suggested by Charpentier *et al.*,[56] the calculated C_Q(^{11}B) value becomes: C_Q(calc) = 2.65 MHz.

Table 4 Experimental and calculated NMR parameters for BBzx. Calculated values reported here are those obtained for the P(1) polymorph (after VASP DFT relaxation of the atomic positions)[49c]

^{1}H NMR			^{13}C NMR			^{11}B NMR						
	δ_{iso} (ppm)			δ_{iso} (ppm)			δ_{iso} (ppm)		C_Q (MHz)		η_Q	
H	Exp	Calc (P(1))	C	Exp[a]	Calc (P(1))	B	Exp[a,b]	Calc (P(1))	Exp[a,b]	Calc (P(1))[c]	Exp[a,b]	Calc (P(1))
H_1	6.3 to 8	7.7	C_1	~130.3	132.9	B_1	31.1	31.6	2.9	3.27	0.48	0.56
H_8		7.8	C_8	~130.3	133.1	B_2		31.5		3.28		0.56
H_2		7.0	C_2	~129.2	131.7							
H_9		7.0	C_9	~129.2	131.7							
H_3	5 to 6.3	6.3	C_3	126.6	128.8							
H_{10}		5.8	C_{10}	127.8	130.3							
H_4		5.6	C_4	~130.3	133.3							
H_{11}		5.7	C_{11}	~129.2	130.9							
H_5	6.3 to 8	7.1	C_5	121.1	121.0							
H_{12}		7.1	C_{12}	121.1	121.0							
H_{7A}	4 to 5	4.5	C_6	153.7	158.8							
H_{14A}		4.6	C_{13}	153.7	159.2							
H_{7B}		4.5	C_7	72.0	73.6							
H_{14B}		4.6	C_{14}	72.0	73.7							

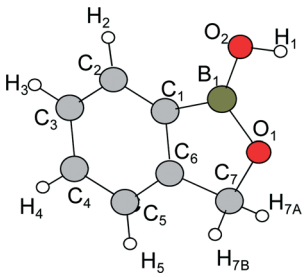

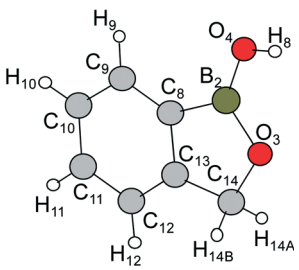

[a] Estimated experimental errors are ~0.2 ppm for δ_{iso}(^{13}C) and δ_{iso}(^{19}F), ~0.1 ppm for δ_{iso}(^{11}B), ~0.02 MHz for C_Q(^{11}B) and ~0.03 for η_Q(^{11}B). [b] Experimental values reported by Bryce *et al.*:[18] C_Q = 2.8 ± 0.1 MHz, η_Q = 0.45 ± 0.10 and δ_{iso} = 31.0 ± 2.0 ppm. [c] Using the scaling factor suggested by Charpentier *et al.*,[56] calculated C_Q(^{11}B) values become: C_Q(calc) = 2.66 and 2.67 MHz.

very close). One point which is worth mentioning at this stage is that for both AN2690 and BBzx, the ^{13}C chemical shifts obtained with the GIPAW calculations are shifted (generally overestimated) compared to the experimental positions (Tables 3 and 4, Fig. S10†). This shift is less pronounced for the methylene carbon but reaches up to ~5 ppm for one of the C atoms of the pentacycle, and up to 9 ppm for the C linked to F. At this stage, we have no interpretation of this shift, and it is a point we are still looking into.

The ^{11}B MAS NMR spectra show very similar lineshapes for both molecules (Fig. 4c). The spectra were simulated considering the presence of a single boron site. The ^{11}B NMR parameters extracted from the fitted lineshapes are very close, with δ_{iso} at ~31.1 ppm, C_Q ~2.8–2.9 MHz and η_Q ~0.48–0.51. It should be noted that in line with previous observations,[18] the two crystallographically independent benzoxaboroles of BBzx cannot be resolved by ^{11}B MAS NMR. For both phases, the experimental δ_{iso} values are found to be in good agreement with the ones calculated by GIPAW, while systematic errors were observed for the ^{11}B quadrupolar parameters, with a systematic overestimation of C_Q. Similar systematic errors have been reported by Bryce and co-workers for boronic acids, when comparing the C_Q(^{11}B) values determined experimentally to those calculated using GIPAW.[55a] It should be noted that Charpentier and co-workers have proposed to apply a scaling factor to the ^{11}B quadrupolar parameters calculated using GIPAW in order to improve the agreement between experimental and calculated values.[56] Here, when applying a similar correction factor, the calculated C_Q values fall closer to the experimental ones.

Finally, the ^{19}F NMR spectrum of AN2690 shows a unique signal centered at ~−108.6 ppm (Fig. 4d), and the experimental chemical shift is in very good agreement with the one calculated by GIPAW. At this stage, only the ^{17}O solid state NMR spectra of BBzx and AN2690 have not been recorded yet, due to the very low natural abundance of oxygen-17. However, based on the results of the GIPAW calculations of ^{17}O NMR parameters (see the ESI,† Tables S7 and S8) and on previous studies in solution,[57] it should be easy to distinguish the two different O atoms of the benzoxaboroles.

Influence of anisotropic thermal expansion and polymorphism on NMR signatures of benzoxaboroles. As mentioned previously, recognizing the crystalline form of a drug is highly important for pharmaceutical applications, as issues like anisotropic thermal expansion properties or polymorphism need to be taken into account and distinguished. Indeed, the physical properties of polymorphs are generally different, with, in some cases, measureable variations in their dissolution properties and bioavailability.[19] In addition to X-ray diffraction, spectroscopic techniques have thus also been developed to characterize cases of polymorphism in molecular materials, such as IR,[58] terahertz spectroscopy,[59] and solid state NMR.[60]

For the small benzoxaborole molecules studied herein, two situations can be distinguished: for BBzx, two polymorphic forms have been described (P(1) and P(2)), while for AN2690, only a single polymorph has been isolated so far, but which presents measureable anisotropic thermal expansion properties (see above). We therefore wondered whether solid state NMR would be sufficiently sensitive to bring evidence of the differences in local environments of BBzx and AN2690 molecules in the different crystalline forms described so far. In order to answer this point, GIPAW calculations of the NMR parameters were carried out on the two polymorphic forms of BBzx and on the two crystal structures of AN2690 (recorded at different temperatures). Results are gathered in Tables S7 and S8 (ESI†).

Concerning BBzx, the calculated ^{1}H, ^{13}C, ^{11}B and ^{17}O NMR parameters of the two polymorphs are nearly identical, which is not fully surprising as the crystal packing is essentially the same in both cases (Table S8 in the ESI†). The minor changes in ^{13}C NMR parameters are all within the error of the uncertainties of the GIPAW calculations, and simulations of the calculated ^{13}C NMR spectra of both polymorphs suggest that it would be impossible to distinguish them unambiguously by ^{13}C solid state NMR.

In the case of AN2690, the anisotropic variations in lattice parameters have a limited impact on the calculated ^{1}H, ^{13}C, ^{17}O and ^{11}B NMR parameters (Table S7 in the ESI†). The only parameter which may be sufficiently sensitive to lead to measurable differences on the solid state NMR spectra (in a reasonable timescale) is the ^{19}F isotropic chemical shift. Indeed, whatever the calculation method used to relax the geometries of both crystalline forms, the ^{19}F chemical shift calculated for the room-temperature structure is lower by at least 0.7 ppm compared to the structure recorded at 100 K. This difference is not biased by the calculation methodology used to perform geometry relaxations, as many different methods were tested (see Table 2), which all led to similar results. Thus, ^{19}F NMR may serve as a probe of the anisotropic thermal expansion of the crystal lattice of AN2690.

To see whether the predicted variations in ^{19}F isotropic shifts with temperature could be observed experimentally, variable-temperature ^{19}F NMR experiments were performed between +20 and −20 °C. While the expected increase in isotropic chemical shifts over that range of frequencies should have been ~0.15 ppm, a decrease of 0.09 ppm was observed experimentally. This shows that the changes in lattice parameters are not the only factors which contribute to the variations in ^{19}F NMR parameters of AN2690 with temperature, and that other parameters such as changes in thermal motion (local dynamics around the atoms) should be considered.[41] As a matter of fact, DFT calculations of vibrational modes of the two AN2690 structures (modeled as infinite periodic systems), show that a difference of 6 cm^{-1} in C–F vibration frequencies can be expected between 293 K and 100 K, indicating that the vibrational properties will indeed be different in both cases, and, as a consequence, the local environment of ^{19}F as well.

All in all, the above study shows how combined experimental-computational studies can help determine whether spectroscopic techniques like solid state NMR can be used (or not) to elucidate cases of polymorphism for benzoxaborole structures in particular. More importantly, for the first time, we also attempted to distinguish the respective influence of temperature-related changes in lattice parameters and of thermal motion on one NMR parameter, the ^{19}F isotropic chemical shift of AN2690. Such considerations should be taken into account more systematically when NMR–crystallography[61] approaches are used to solve crystal structures, and when discrepancies between experimental and calculated NMR parameters are attributed to temperature effects.[55c,62]

4. Conclusion

In this manuscript, we have shown how the combination of several characterization techniques (including multinuclear solid state NMR) and DFT computational modeling (involving calculations of IR and NMR spectral signatures) is necessary to understand in detail the crystal structure of simple benzoxaborole molecules, such as those currently being studied for pharmaceutical applications. Particular emphasis was made on the importance of taking into account temperature effects, as we have shown how polymorphism and anisotropic thermal expansion can influence not only XRD powder patterns but also solid state NMR spectra. Thus, this work should help in the development of more precise "NMR crystallography" approaches, by shedding light on the different parameters which can affect the NMR spectra of molecular crystals and which can lead to discrepancies between experimental and calculated parameters. Beyond the study of the

BBzx and AN2690 molecules, this work will be useful for the investigation of complex materials containing benzoxaboroles, especially in cases where techniques complementary to X-ray diffraction (such as solid state NMR) are needed to fully elucidate their structure. We are currently looking into this direction, through the development of hybrid materials involving benzoxaboroles, and using solid state NMR techniques to elucidate structural issues.

Acknowledgements

The authors acknowledge the CNRS and the Agence Nationale de la Recherche (ANR "BOROMAT" project) for funding. This work was granted access to the HPC resources of CINES (Jade) under the allocations C2013076866 and C2014076866 made by GENCI (Grand Equipement National de Calcul Intensif) for geometry optimizations and IR calculations. NMR spectroscopic calculations were performed on the IDRIS supercomputer centre of the CNRS (project: 091461). Further details on the computation method can be provided on demand. Dr J.-P. Flament is acknowledged for his assistance in the PED analyses.

Notes and references

1 D. G. Hall, *Boronic Acids: Preparation and Applications in Organic Synthesis Medicine and Materials*, Wiley-VCH, Weinheim, 2011.
2 A. J. J. Lennox and G. C. Lloyd-Jones, *Chem. Soc. Rev.*, 2014, **43**, 412.
3 (*a*) R. Nishiyabu, Y. Kubo, T. D. James and J. S. Fossey, *Chem. Commun.*, 2011, **47**, 1106; (*b*) R. Nishiyabu, Y. Sugino and Y. Kubo, *Chem. Commun.*, 2013, **49**, 9869.
4 (*a*) S. Y. Ding and W. Wang, *Chem. Soc. Rev.*, 2013, **42**, 548; (*b*) R. Nishiyabu, Y. Kubo, T. D. James and J. S. Fossey, *Chem. Commun.*, 2011, **47**, 1124.
5 (*a*) R. Smoum, A. Rubinstein, V. M. Dembitsky and M. Srebnik, *Chem. Rev.*, 2012, **112**, 4156; (*b*) P. V. Ramachandran, *Future Med. Chem.*, 2013, **5**, 611 (and references therein).
6 S. J. Baker, J. W. Tomsho and S. J. Benkovic, *Chem. Soc. Rev.*, 2011, **40**, 4279.
7 (*a*) S. J. Baker, Y.-K. Zhang, T. Akama, A. Lau, H. Zhou, V. Hernandez, W. Mao, M. R. K. Alley, V. Sanders and J. J. Plattner, *J. Med. Chem.*, 2006, **49**, 4447; (*b*) X. Hui, S. J. Baker, R. C. Wester, S. Barbadillo, A. K. Cashmore, V. Sanders, K. M. Hold, T. Akama, Y.-K. Zhang, J. J. Plattner and H. I. Maibach, *J. Pharm. Sci.*, 2007, **96**, 2622.
8 (*a*) T. Akama, S. J. Baker, Y.-K. Zhang, V. Hernandez, H. Zhou, V. Sanders, Y. Freund, R. Kimura, K. R. Maples and J. J. Plattner, *Bioorg. Med. Chem. Lett.*, 2009, **19**, 2129; (*b*) R. T. Jacobs, B. Nare, S. A. Wring, M. D. Orr, D. Chen, J. M. Sligar, M. X. Jenks, R. A. Noe, T. S. Bowling, L. T. Mercer, C. Rewerts, E. Gaukel, J. Owens, R. Parham, R. Randolph, B. Beaudet, C. J. Bacchi, N. Yarlett, J. J. Plattner, Y. Freund, C. Ding, T. Akama, Y.-K. Zhang, R. Brun, M. Kaiser, I. Scandale and R. Don, *PLoS Neglected Trop. Dis.*, 2011, **5**, e1151; (*c*) T. Akama, C. Dong, C. Virtucio, Y. R. Freund, D. Chen, M. D. Orr, R. T. Jacobs, Y.-K. Zhang, V. Hernandez, Y. Liu, A. Wu, W. Bu, L. Liu, K. Jarnagin and J. J. Plattner, *Bioorg. Med. Chem. Lett.*, 2013, **23**, 5870.
9 http://www.anacor.com.
10 (*a*) C. T. Liu and S. J. Benkovic, *J. Am. Chem. Soc.*, 2013, **135**, 14544; (*b*) S. Biswas, K. Kinbara, T. Niwa, H. Taguchi, N. Ishii, S. Watanabe, K. Miyata, K. Kataoka and T. Aida, *Nat. Chem.*, 2013, **5**, 613; (*c*) G. A. Ellis, M. J. Palte and R. T. Raines, *J. Am. Chem. Soc.*, 2012, **134**, 3631; (*d*) J. W. Tomsho and S. J. Benkovic, *J. Org. Chem.*, 2012, **77**, 11200; (*e*) Y. Kotsuchibashi, R. V. C. Agustin, J.-Y. Lu, D. G. Hall and R. Narain, *ACS Macro Lett.*, 2013, **2**, 260.
11 (*a*) A. Adamczyk-Wozniak, M. K. Cyranski, A. Zubrowska and A. Sporzynski, *J. Organomet. Chem.*, 2009, **694**, 3533; (*b*) E. Jaskowska, I. Justyniak, M. K. Cyranski, A. Adamczyk-Wozniak, A. Sporzynski, E. Zygado-Monikowska and W. Ziemkowska, *J. Organomet. Chem.*, 2013, **732**, 8.
12 J. Zhang, M. Y. Zhu, Y. N. Lin and H. C. Zhou, *Sci. China: Chem.*, 2013, **56**, 1372.
13 J. W. Tomsho, A. Pal, D. G. Hall and S. J. Benkovic, *ACS Med. Chem. Lett.*, 2012, **3**, 48.
14 A. Jezierska, J. J. Panek, G. Z. Zukowskac and A. Sporzynski, *J. Phys. Org. Chem.*, 2010, **23**, 451.
15 I. D. Madura, A. Adamczyk-Wozniak, M. Jakubczyk and A. Sporzynski, *Acta Crystallogr., Sect. E: Struct. Rep. Online*, 2011, **67**, 414.
16 V. V. Zhdankin, P. J. Persichini III, L. Zhang, S. Fix and P. Kiprof, *Tetrahedron Lett.*, 1999, **40**, 6705.
17 A. Adamczyk-Wozniak, M. K. Cyranski, M. Jakubczyk, P. Klimentowska, A. Koll, J. Kołodziejczak, G. Pojmaj, A. Zubrowska, G. Z. Zukowska and A. Sporzynski, *J. Phys. Chem. A*, 2010, **114**, 2324.
18 J. W. E. Weiss and D. L. Bryce, *J. Phys. Chem. A*, 2010, **114**, 5119.
19 (*a*) J.-P. Brog, C.-L. Chanez, A. Crochet and K. M. Fromm, *RSC Adv.*, 2013, **3**, 16905; (*b*) J. Bernstein, *Cryst. Growth Des.*, 2011, **11**, 632; (*c*) M. Bauer, *Tech. Ing.*, 2005, P 1098.
20 *CrysAlisPro*, Agilent Technologies, Vers 1.171.36.24'Version 1.171.34.40.
21 SCALE3 ABSPACK scaling algorithm.
22 M. C. Burla, R. Caliandro, M. Camalli, B. Carrozzini, G. L. Cascarano, L. De Caro, C. Giacovazzo, G. Polidori and R. Spagna, *J. Appl. Crystallogr.*, 2005, **38**, 381.
23 G. M. Sheldrick, 1997, *SHELXL-97. Program for Crystal Structure Refinement*, University of Gottingen, Germany.
24 L. J. Farrugia, *J. Appl. Crystallogr.*, 2012, **45**, 849.
25 (*a*) M. Leskes, P. K. Madhu and S. Vega, *Chem. Phys. Lett.*, 2007, **447**, 370; (*b*) D. Sakellariou, A. Lesage, P. Hodgkinson and L. Emsley, *Chem. Phys. Lett.*, 2000, **319**, 253; (*c*) A. Lesage, D. Sakellariou, S. Hediger, B. Elena, P. Charmont, S. Steuernagel and L. Emsley, *J. Magn. Reson.*, 2003, **163**, 105.
26 *Gaussian 09, Revision D.01*, M. J. Frisch, G. W. Trucks, H. B. Schlegel, G. E. Scuseria, M. A. Robb, J. R. Cheeseman, G. Scalmani, V. Barone, B. Mennucci, G. A. Petersson,

H. Nakatsuji, M. Caricato, X. Li, H. P. Hratchian, A. F. Izmaylov, J. Bloino, G. Zheng, J. L. Sonnenberg, M. Hada, M. Ehara, K. Toyota, R. Fukuda, J. Hasegawa, M. Ishida, T. Nakajima, Y. Honda, O. Kitao, H. Nakai, T. Vreven, J. A. Montgomery Jr., J. E. Peralta, F. Ogliaro, M. Bearpark, J. J. Heyd, E. Brothers, K. N. Kudin, V. N. Staroverov, R. Kobayashi, J. Normand, K. Raghavachari, A. Rendell, J. C. Burant, S. S. Iyengar, J. Tomasi, M. Cossi, N. Rega, J. M. Millam, M. Klene, J. E. Knox, J. B. Cross, V. Bakken, C. Adamo, J. Jaramillo, R. Gomperts, R. E. Stratmann, O. Yazyev, A. J. Austin, R. Cammi, C. Pomelli, J. W. Ochterski, R. L. Martin, K. Morokuma, V. G. Zakrzewski, G. A. Voth, P. Salvador, J. J. Dannenberg, S. Dapprich, A. D. Daniels, Ö. Farkas, J. B. Foresman, J. V. Ortiz, J. Cioslowski and D. J. Fox, Gaussian, Inc., Wallingford CT, 2009.

27 (*a*) A. D. Becke, *J. Phys. Chem.*, 1993, **98**, 5648; (*b*) C. Lee, W. Yang and R. Parr, *Phys. Rev. B: Condens. Matter Mater. Phys.*, 1988, **37**, 785.

28 B. Xerri, J.-P. Flament, H. Petitjean, C. Berthomieu and D. Berthomieu, *J. Phys. Chem. B*, 2009, **113**, 15119 (and references therein).

29 M. Tadjeddine and J.-P. Flament, *Chem. Phys.*, 2001, **265**, 27.

30 S. J. Hickling and R. G. Wooleey, *Chem. Phys. Lett.*, 1990, **166**, 43.

31 G. Kresse and J. Hafner, *J. Phys.: Condens. Matter*, 1994, **6**, 8245.

32 R. Dovesi, V. R. Saunders, C. Roetti, R. Orlando, C. M. Zicovich-Wilson, F. Pascale, B. Civalleri, K. Doll, N. M. Harrison, I. J. Bush, P. D. Arco and M. Llunell, *CRYSTAL09 Users Manual*, University of Turin, Turin, 2009, see http://www.crystal.unito.it.

33 P. Giannozzi, S. Baroni, N. Bonini, M. Calandra, R. Car, C. Cavazzoni, D. Ceresoli, G. L Chiarotti, M. Cococcioni, I. Dabo, A. Dal Corso, S. de Gironcoli, S. Fabris, G. Fratesi, R. Gebauer, U. Gerstmann, C. Gougoussis, A. Kokalj, M. Lazzeri, L. Martin-Samos, N. Marzari, F. Mauri, R. Mazzarello, S. Paolini, A. Pasquarello, L. Paulatto, C. Sbraccia, S. Scandolo, G. Sclauzero, A. P Seitsonen, A. Smogunov, P. Umari and R. M Wentzcovitch, Quantum Espresso: A Modular and Open-Source Software Project for Quantum Simulations of Materials., *J. Phys.: Condens. Matter*, 2009, **21**, 395502.

34 S. Grimme, *J. Comput. Chem.*, 2006, **27**, 1787.

35 B. Civalleri, C. M. Zicovich-Wilson, L. Valenzano and P. Ugliengo, *CrystEngComm*, 2008, **10**, 405.

36 M. F. Peintinger, D. Vilela Oliveira and T. Bredow, *J. Comput. Chem.*, 2013, **34**, 451.

37 J. P. Perdew, K. Burke and M. Ernzerhof, *Phys. Rev. Lett.*, 1996, **77**, 3865.

38 G. Kresse and D. Joubert, *Phys. Rev. B: Condens. Matter Mater. Phys.*, 1999, **59**, 1758.

39 (*a*) N. Troullier and J. L. Martins, *Phys. Rev. B: Condens. Matter Mater. Phys.*, 1991, **43**, 1993; (*b*) L. Kleinman and D. Bylander, *Phys. Rev. Lett.*, 1982, **48**, 1425.

40 C. J. Pickard and F. Mauri, *Phys. Rev. B: Condens. Matter Mater. Phys.*, 2001, **63**, 245101.

41 T. Charpentier, *Solid State Nucl. Magn. Reson.*, 2011, **40**, 1.

42 (*a*) C. Bonhomme, C. Gervais, F. Babonneau, C. Coelho, F. Pourpoint, T. Azaïs, S. E. Ashbrook, J. M. Griffin, J. R. Yates, F. Mauri and C. J. Pickard, *Chem. Rev.*, 2012, **112**, 5733; (*b*) C. Bonhomme, C. Gervais and D. Laurencin, *Prog. Nucl. Magn. Reson. Spectrosc.*, 2014, **77**, 1.

43 C. Gervais, M. Profeta, V. Lafond, C. Bonhomme, T. Azaïs, H. Mutin, C. J. Pickard, F. Mauri and F. Babonneau, *Magn. Reson. Chem.*, 2004, **42**, 445.

44 P. Pyykkö, *Mol. Phys.*, 2008, **106**, 1965.

45 (*a*) M. Biswal, M. Body, C. Legein, A. Sadoc and F. Boucher, *J. Solid State Chem.*, 2013, **207**, 208; (*b*) M. Body, C. Legein, M. Biswal, F. Fayon, X. Rocquefelte and F. Boucher, *Phys. Chem. Chem. Phys.*, 2011, **13**, 18539.

46 D. S. Gunasekera, D. J. Gerold, N. S. Aalderks, J. S. Chandra, C. A. Maanu, P. Kiprof, V. V. Zhdankin and M. V. Ram Reddya, *Tetrahedron*, 2007, **63**, 9401.

47 C. Z. Ding, Y.-K. Zhang, X. Li, Y. Liu, S. Zhang, Y. Zhou, J. J. Plattner, S. J. Baker, L. Liu, M. Duan, R. L. Jarvest, J. Ji, W. M. Kazmierski, M. D. Tallant, L. L. Wright, G. K. Smith, R. M. Crosby, A. A. Wang, Z.-J. Ni, W. Zou and J. Wright, *Bioorg. Med. Chem. Lett.*, 2010, **20**, 7317.

48 B. Frode Lutnaes, G. Luthe, U. A. Th. Brinkman, J. E. Johansen and J. Krane, *Magn. Reson. Chem.*, 2005, **43**, 588.

49 (*a*) CCDC 811360; (*b*) CCDC 744739; (*c*) CSD LOQQEN.

50 (*a*) M. A. Spackman and D. Jayatilaka, *CrystEngComm*, 2009, **11**, 19; (*b*) M. A. Spackman and J. J. McKinnon, *CrystEngComm*, 2002, **4**, 378; (*c*) *CrystalExplorer (Version 3.1)*, S. K. Wolff, D. J. Grimwood, J. J. McKinnon, M. J. Turner, D. Jayatilaka and M. A. Spackman, University of Western, Australia, 2012.

51 (*a*) G. A. Stephenson, *J. Pharm. Sci.*, 2006, **95**, 821; (*b*) D. Das, T. Jacobs and L. J. Barbour, *Nat. Mater.*, 2010, **9**, 36.

52 G. Kaur, P. Panini, D. Chopra and A. Roy Choudhury, *Cryst. Growth Des.*, 2012, **12**, 5096.

53 GIPAW calculations were performed by keeping lattice parameters constant, starting from high quality single-crystal XRD structures. In this sub-section, for AN2690, the lattice parameters (and the XRD structure) deriving from the room-temperature structure solved here were used, while for BBzx, those previously reported for the P(1) polymorph were used.

54 F. Pourpoint, C. Gervais, L. Bonhomme-Coury, T. Azaïs, C. Coelho, F. Mauri, B. Alonso, F. Babonneau and C. Bonhomme, *Appl. Magn. Reson.*, 2007, **32**, 435.

55 (*a*) S.-W. Oh, J. W. E. Weiss, P. A. Kerneghan, I. Korobkov, K. E. Maly and D. L. Bryce, *Magn. Reson. Chem.*, 2012, **50**, 388; (*b*) M. Reinholdt, J. Croissant, L. Di Carlo, D. Granier, P. Gaveau, S. Bégu, J.-M. Devoisselle, P. H. Mutin, M. E. Smith, C. Bonhomme, C. Gervais, A. van der Lee and D. Laurencin, *Inorg. Chem.*, 2011, **50**, 7802; (*c*) S. Sene, M. Reinholdt, G. Renaudin, D. Berthomieu, C. M. Zicovich-Wilson, C. Gervais, P. Gaveau, C. Bonhomme, Y. Filinchuk, M. E. Smith, J.-M. Nedelec, S. Begu, P. H. Mutin and D. Laurencin, *Chem. – Eur. J.*, 2013, **19**, 880.

56 A. Soleilhavoup, J. M. Delaye, F. Angeli, D. Caurant and T. Charpentier, *Magn. Reson. Chem.*, 2010, **48**, S159.
57 A. Adamczyk-Wozniak, K. M. Borys, I. D. Madura, A. Pawełko, E. Tomecka and K. Zukowski, *New J. Chem.*, 2013, **37**, 188.
58 J. Li, S. A. Bourne, M. M. de Villiers, A. M. Crider and M. R. Caira, *Cryst. Growth Des.*, 2011, **11**, 4950.
59 S. Pellizzeri, S. P. Delaney, T. M. Korter and J. Zubieta, *J. Phys. Chem. A*, 2014, **118**, 417.
60 J. C. Burley, M. J. Duer, R. S. Stein and R. M. Vrcelj, *Eur. J. Pharm. Sci.*, 2007, **31**, 271.
61 (*a*) R. K. Harris, R. E. Wasylishen and M. J. Duer, *NMR Crystallography*, Wiley-VCH, Weinheim, 2009; (*b*) J. A. Ripmeester and R. E. Wasylishen, *CrystEngComm*, 2013, **15**, 8598 (and references therein: special issue on NMR crystallography).
62 (*a*) E. Davies, M. J. Duer, S. E. Ashbrook and J. M. Griffin, *J. Am. Chem. Soc.*, 2012, **134**, 12508; (*b*) A. L. Webber, B. Elena, J. M. Griffin, J. R. Yates, T. N. Pham, F. Mauri, C. J. Pickard, A. M. Gil, R. Stein, A. Lesage, L. Emsley and S. P. Brown, *Phys. Chem. Chem. Phys.*, 2010, **12**, 6970.